Particle
& Particle Systems Characterization
www.particle-journal.com

Materials Views
www.MaterialsViews.com

Silver-Based Nanoparticles for Surface Plasmon Resonance in Organic Optoelectronics

Su-Hun Jeong, Hyosung Choi, Jin Young Kim, and Tae-Woo Lee**

Organic optoelectronic devices including organic light-emitting diodes (OLEDs) and polymer solar cells (PSCs) have many advantages, including low-cost, mechanical flexibility, and amenability to large-area fabrication based on printing techniques, and have therefore attracted attention as next-generation flexible optoelectronic devices. Although almost 100% internal quantum efficiency of OLEDs has been achieved by using phosphorescent emitters and optimizing device structures, the external quantum efficiency (EQE) of OLEDs is still limited due to poor light extraction. Also, although intensive efforts to develop new conjugated polymers and device architectures have improved power conversion efficiency (PCE) up to 8%–9%, device efficiency must be improved to >10% for commercialization of PSCs. The surface plasmon resonance (SPR) effect of metal nanoparticles (NPs) can be an effective way to improve the extraction of light produced by decay of excitons in the emission layer and by absorption of incident light energy within the active layer. Silver (Ag) NPs are promising plasmonic materials due to a strong SPR peak and light-scattering effect. In this review, different SPR properties of Ag NPs are introduced as a function of size, shape, and surrounding matrix, and review recent progress on application of the SPR effect of AgNPs to OLEDs and PSCs.

1. Introduction

Organic optoelectronic devices including organic light-emitting diodes (OLEDs) and polymer solar cells (PSCs) are promising candidates for next-generation flexible and stretchable optoelectronic devices.[1,2] The devices have attracted great attention due to advantages such as low cost, solution processability, and feasibility of large-area fabrication on flexible and stretchable substrates.[3–6] Significant efforts to synthesize new organic materials, to develop device architectures, and to control the morphology of organic layers, have improved the efficiencies of PSCs to 10%[7–15] and the panel efficiency of white OLEDs to 110 lm W^{-1}.[16,17] This rapid progress offers the possibility for OLEDs and PSCs to be next-generation flexible organic optoelectronic devices with low cost and high efficiency.

OLEDs have received great attention as potential next-generation displays due to their low power consumption, excellent color gamut, fast response time, and especially their flexibility.[18] Although almost 100 % internal quantum efficiency of OLEDs has been achieved by using phosphorescent emitters and optimized device structures,[19] the external quantum efficiency (EQE) is still limited due to poor light extraction.[16,18,20] The key challenge is to improve the extraction of light trapped between layers and the energy transfer between donor and acceptor molecules in emissive layers.

The power conversion efficiency (PCE) improvement of PSCs is mostly dependent on the development of new conjugated polymers and device structures. At present, an important challenge is to find effective ways to further improve the performance of PSCs in conjunction with novel materials and device architectures. One simple strategy to achieve high device efficiency is to increase the light absorption within the active layer by producing a thick active layer, thereby improving short-circuit current density. However, exciton diffusion length and charge-carrier mobility of organic materials are in the range of 1–10 nm and 10^{-5} –10 cm^2 V^{-1} s^{-1}, respectively.[21–26] As a result, although a thick active layer can absorb many photons, considerable recombination loss can occur during exciton diffusion, dissociation, and charge transport.[27,28] Specifically, regulating the thickness of active layer entails a trade off between photogenerated charge-carrier efficiency and collection efficiency.[29] The key goal is to reduce the physical thickness of the active layer while maintaining its optical thickness.[30]

One useful strategy for light trapping and emitting in PSCs and OLEDs is to exploit the surface plasmon resonance (SPR) effect of metal nanostructures. Surface plasmons are collective oscillations of free electrons at the interface between the metal and dielectric.[31–33] The SPR effect, which is induced by an electric field at specific incident wavelength, leads to intense surface plasmon absorption bands and strong light scattering with concurrent strengthening of local electromagnetic fields.[30,34] By exploiting either localized surface plasmons (LSPs) excited in metal nanoparticles (NPs) or surface plasmon polaritons (SPPs)

S.-H. Jeong, Prof. T.-W. Lee
Department of Materials Science and Engineering
Pohang University of Science
and Technology (POSTECH)
Pohang, Gyungbuk 790–784, South Korea
E-mail: twlee@postech.ac.kr
H. Choi, Prof. J. Y. Kim
Department of Energy
Ulsan National Institute of Science and Technology (UNIST)
Ulsan 689–798, South Korea
E-mail: jykim@unist.ac.kr

DOI: 10.1002/ppsc.201400117

propagating at the interface between metal and semiconductor, the light can be efficiently concentrated into a thin active layer, thereby maximizing the light absorption. In particular, metal NPs function as effective subwavelength antennas and scattering elements to store the incident energy in LSP modes and to increase the optical path length of the incident light within the active layer, leading to photogeneration of charge-carriers in PSCs (**Figure 1**).[29,30] In addition, metal NPs are easily applicable to OLEDs and PSCs by means of solution processing.[35–37]

In this review, we focus on an efficient light-trapping and -emitting approach using the SPR effect of silver NPs (Ag NPs) to fabricate high-performance plasmonic OLEDs and PSCs because of many advantages of Ag NPs compared to other metal NPs.

2. Unique Properties of Nanoparticles

Ag NPs constitute a promising plasmonic nanomaterial because of their many advantages. We will discuss the merits of Ag NPs and their unique SPR effects depending on size, shape, elemental composition, and surround matrix in the next subsections.

2.1. Advantages of Silver Nanoparticles

Among various metal NPs, Ag NPs have exhibited the most effective light trapping potential due to their strong light scattering and surface plasmon (SP) strength.[38–40] In addition, SPR absorption spectra of silver nanoparticles (Ag NPs) can be controlled from 300 (ultraviolet (UV)) to 1200 nm (near-infrared (NIR)). The ability of metal NPs for SPR effect depends on its dielectric function ε including a real part ε_r and an imaginary part ε_i, both of which vary with excitation wavelength λ.[40]

The SPR effect of metal NPs with spherical structure can be described using the extinction (absorption + scattering) cross-section based on Mie theory,[41]

$$C_{ext} = \frac{24\pi^2 R^3 \varepsilon_m^{3/2}}{\lambda}\left[\frac{\varepsilon_i}{(\varepsilon_r + 2\varepsilon_m)^2 + \varepsilon_i^2}\right] \quad (1)$$

where C_{ext} is the extinction cross-section, R is the NP radius, and ε_m is the relative dielectric constant of the matrix surrounding the metal NPs. This equation implies that dielectric properties have strong effect on the interaction between light and metal NPs. In addition, the SP strength (or damping) of metal NPs can be expressed using the quality factor (QF),[42]

$$\mathrm{QF} = \frac{w\left(d\varepsilon_r / dw\right)}{2(\varepsilon_i)^2} \quad (2)$$

SP strength is proportional to QF. Specifically, high QF indicates strong plasmons and low QF means weak SP with a small C_{ext}. Ag has higher QF than do other metals over the spectrum from 300 to 1200 nm. Interband transitions (IBTs), which are excitations of electrons from the conduction band to higher energy levels, are key factor for the SP strength.[43] In Ag, these transitions occur at much higher energies than the SPR, whereas these transitions limit their SPR excitation to wavelength >500 nm for Au and >600 nm for Cu.[44,45] Taking into account, these factors and others including plasmonic ability,

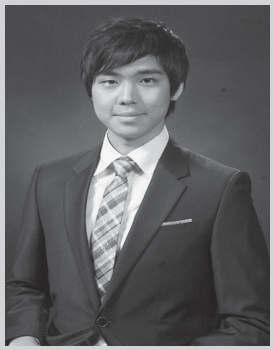

Su-Hun Jeong received his B.S. in the Department of Materials Science and Engineering in 2012 from Pohang University of Science and Technology (POSTECH). He is a graduate student in POSTECH since 2010. His current research work is focused on polymeric electrodes for flexible organic optoelectronic devices.

Jin Young Kim is an associate professor in the Department of Energy Engineering, Ulsan National University of Science and Technology, Ulsan, Korea (July 2008–present). He received his Ph.D. in physics from Pusan National University (September 2000–February 2005). He served as an assistant research professor, in the Heeger Center for Advanced Materials, Gwangju Institute of Science and Technology (GIST), Gwangju, Korea (July 2007–2008) and he was a postdoctoral researcher, in the Center for Polymers and Organic Solids, UC Santa Barbara, Santa Barbara, USA (April 2005–July 2007). His research interests include organic and hybrid solar cells, and energy-related devices.

Tae-Woo Lee is an associate professor in the Department of the Materials Science and Engineering at POSTECH, Korea. He received his Ph.D. in chemical engineering from KAIST, Korea in February 2002. Then, he joined Bell Laboratories, USA as a postdoctoral researcher in 2002. From September 2003 to August 2008, he worked in Samsung Advanced Institute of Technology as a member of research staff. He received a prestigious Korea Young Scientist Award from the President of Korea in 2008 and The Scientist of the Month Award from the ministry of science, ICT and future planning in 2013. His research focuses on printed and organic electronics based on organic and carbon materials for flexible electronics, displays, solid-state lightings, and solar energy conversion devices.

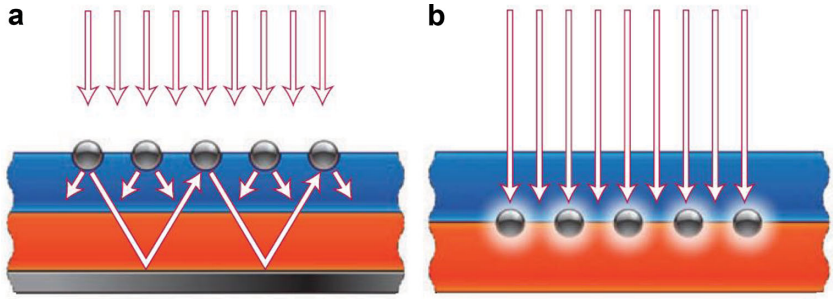

Figure 1. Plasmonic light-trapping mechanism of metal NPs: a) light trapping by scattering from metal NPs at the surface of the device. b) Light trapping by the excitation of SPs in metal NPs embedded in semiconductor. Reproduced with permission.[29] Copyright 2010, NPG.

material cost, and chemical stability, Ag is the most economical and effective candidate for plasmonic applications (**Table 1**).[40]

2.2. Photoluminescence Enhancement Mediated by Surface Plasmon Resonance of Silver Nanoparticles

Photoluminescence (PL) is a process in which a photoexcited material releases its energy as light.[46] Ag NPs have been reported to cause radiative enhancement when they have a certain size and are kept at a certain distance from emissive molecules.[47–51] This enhancement can come from enhanced resonance-energy transfer or from near-field enhancement by the interactions of the emissive molecules with the SPR effect of Ag NPs in a certain wavelength of incident light. LSPs of Ag nanoparticles and propagating surface plasmons of Ag nanofilms increase PL from a conjugated polymer, poly[2-methoxy-5-(2-ethylhexyloxy)-1,4-phenylenevinylene] (MEH-PPV); changing the Ag nanostructures from NPs to nanofilms by increasing the thickness of deposited Ag yielded large PL enhancement of a MEH-PPV film.[52] Both surface localized and propagating surface plasmons contributed to the enhanced PL.

SPR-enhanced radiative emission can be used to enhance Förster resonance energy transfer (FRET)[47–49] between donor and acceptor molecules; In FRET, the energy of excited donor molecules is transferred to neighboring acceptor molecules by nonradiative dipole–dipole interaction (**Figure 2**).[53,54] This energy transfer decreases the donor emission intensity, thereby reducing the donor lifetime, and enhances the acceptor emission intensity. When the SPR wavelength of Ag NPs overlaps the wavelengths of donor emission and acceptor absorption, FRET from donor to acceptor molecules can be increased by improving donor emission and acceptor absorption.[49,50]

The SPR effect-mediated energy transfer enhancement is greatly influenced by the shape, size and SPR wavelength of noble metal nanostructures, and by the position of the donor–acceptor pair relative to nanostructures.[49] The SPR effect of Au–Ag core–shell NRs affects FRET.[47] The energy transfer efficiency E can be calculated from the energy transfer rate k_{ET} and the sum k_D of the donor's radiative and non-radiative decay rates:

$$E = \frac{k_{ET}}{k_D + k_{ET}} \quad (3)$$

When the SPR peak overlaps the donor emission peak, k_D increases but k_{ET} does not, so E decreases. When the SPR peak is between the donor emission peak and the acceptor absorption peak, k_{ET} increases and consequently E increases.

2.3. Surface Plasmon Resonance Effect of Silver Nanoparticles Depending on Size, Shape, Elemental Composition, and Surrounding Matrix

The SPR effect is collective oscillation of valance electrons that is induced by resonant photons when their frequency matches the natural frequency of surface electrons. Different noble metals have different resonant photon frequencies. Ag NPs have resonant wavelengths in UV–vis (vis) region. The resonant wavelength and SPR intensity of Ag NPs are dependent on their,[55,56] shape,[57–59] elemental composition (alloy, core–shell),[60–62] and surrounding matrix.[63–65]

The size of Ag NPs affects the SPR absorption peak and intensity as well as light scattering. For large Ag NPs, the scattering effect is more dominant than light absorption; furthermore, increasing the size resulted in red-shift of the SPR peak and broadening of the absorption band (**Figure 3**a).[55,56] Ag nanocubes have the same tendencies as Ag NPs. Ag nanocubes exhibited continuous red-shift and broadening of SPR peaks as their edge length was increased from 36 to 172 nm.[66]

The shapes of Ag NPs strongly affect their plasmonic properties. Changing the sharpness of the edges of Ag NPs affects their UV–vis extinction spectra[58] (Figure 3b). The SPR absorption bands of Ag NPs steadily blue-shifts the Ag NP shape

Table 1. Comparison of characteristics of various metals for plasmonic applications. Table reproduced with permission.[40] Copyright 2011, ACS.

Metal	Cost [$/ounce]	Plasmonic ability	Nanostructure formations	Chemical stability
Aluminum	0.049	Good in UV region	Few	Stable after surface passivation
Silver	13.4	Highest in QF	Many	Oxidation
Copper	14.8	IBT below 600 nm	Few	Easy oxidation
Palladium	265	Low QF	Many	Stable
Gold	950	IBT below 600 nm, high QF	Many	Very stable
Platinum	1207	Low QF	Many	Stable

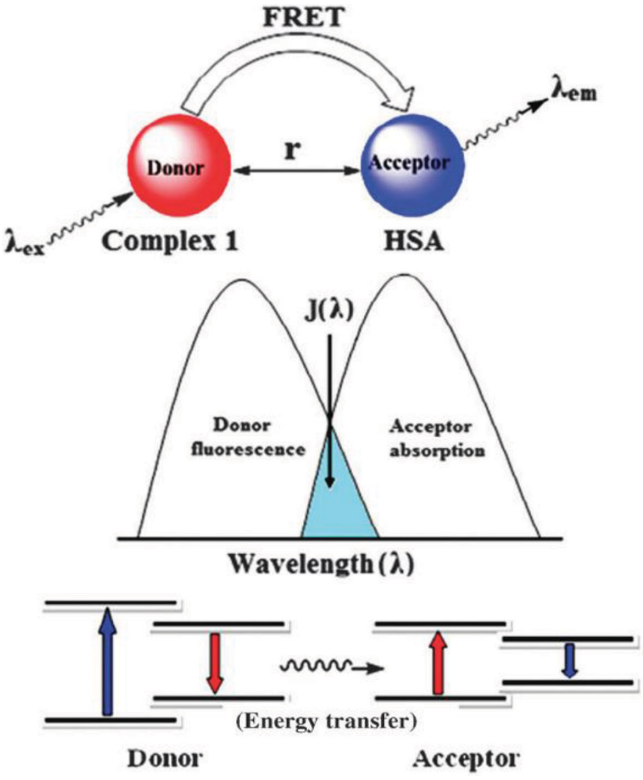

Figure 2. Schematic of Förster resonance energy transfer (FRET). Reproduced with permission.[54] Copyright 2012, The Royal Society of Chemistry.

changes from triangular nanoplates to circular disks. Specifically, Ag NPs with sharp edges have red-shifted extinction spectra compared to those of Ag NPs with rounded structures because the sharp nature of the Ag NPs tends to increase charge separation and to reduce the restoring force for the dipole oscillation.

The shapes (e.g., sphere, cube, octahedron, and right bipyramid) of Ag NPs also can affect their extinction spectra.[59] Ag spheres only have one SPR peak at 410 nm, whereas Ag cubes have a strong SPR peak at 450 nm and a few shoulders. Compared to Ag spheres, Ag cubes, octahedra, and right bipyramids have lower symmetry, leading to polarization of electrons in multiple directions. In short, the number of SPR peaks increases with the number of ways in which it can be polarized and the SPR peaks red-shift with increasing corner sharpness and anisotropy.

The geometry of Ag NPs can change the position of the SPR peak. The Ag NPs with sphere and cube structure have sharp dipole resonances that dominate the spectra. Compared to the SPR peak of Ag spheres, SPR peaks of Ag NPs with cube, octahedron, and right bipyramid structures are red-shifted about 40, 50, and 100 nm, respectively. Greater charge separation occurred by sharp corners of the cubic structure during dipole oscillation, leading to reduced restoring force and consequently longer resonance wavelength.

Alloying and developing core–shell structure are effective strategies for tuning SPR properties of Ag NPs. Various Ag-based alloys can be synthesized by using different metal types and compositions such as Ag–Au,[67,68] Ag–Pt,[69,70] and Ag–Pd.[69] One representative alloy structure is an Ag–Au alloy nanocage synthesized by galvanic reaction.[71] The SPR peak of these alloy nanocages can be tuned from visible to NIR by varying the Ag/Au ratio. Various types of core–shell metal NPs have been reported including Ag–Au,[72,73] Au–Ag,[74,75] and Ag-Cu.[76,77]

Core–shell metal NPs have unique SPR properties compared to mixtures of pure metal NPs. The mixture of Ag and Au NPs has SPR peaks at 400 and 520 nm, which correspond to the plasmonic peak of pure Ag NPs and pure Au NPs, respectively.[78] In contrast, Ag–Au core–shell metal NPs have only one SPR peak at 500 nm with a broad shoulder at 400 nm.[79] This core–shell structure can be used together with the strategy of controlling the shape of metal NCs. One example is use of Au–Ag core–shell nanorods (NRs).[62] The extinction spectra of Au–Ag core–shell NRs can be tailored from visible to NIR by varying the Au core size and the Ag shell thickness. Pure Au NRs have transverse and longitudinal plasmon resonance wavelengths at 512 and 868 nm, respectively; increasing the thickness of Ag shell resulted in blue-shift of SPR peaks from Au NRs, and new resonance peaks from Ag shell appeared after the Ag shell reached a certain thickness (Figure 3c). These multiple plasmonic peaks may be attributed to synergic effects of bimetallic and asymmetric properties of Au–Ag core–shell NRs. This strategy of coating Ag NPs with different materials can eliminate the reactivity and toxicity of Ag.[80,81]

The SPR properties of Ag NPs can be tuned by engineering the dielectric constant of the surrounding matrix. In general, small Ag NPs in air have an SPR peak at 400 nm.[30] Different surrounding matrixes (including SiO_2, Si_3N_4, Si, TiO_2) cause the peak to red-shift over the entire 500–1000 nm due to the change of dielectric constant (Figure 2d).[65] Surrounding metal NPs with a dielectric layer hinders direct quenching between metal NPs and semiconductors, and is therefore a useful way to prevent exciton quenching.[61]

3. Recent Progress in Plasmonic Organic Light-Emitting Diodes using Silver Nanoparticles

OLEDs have received great attention as a next-generation display due to their notable properties, especially flexibility.[82] Although almost 100% internal quantum efficiency of OLEDs has been achieved by using phosphorescent emitters and optimizing device structures,[19] EQE is still limited due to the poor light extraction.[20] The large difference between the refractive indices n of the air ($n = 1$), glass ($n \approx 1.5$), indium tin oxide (ITO) ($n \approx 2.0$), and organic layer ($n \approx 1.7$–2) trap the emitted light in the ITO/organic layer and ITO/glass as wave guide modes. The large refractive index differences of layers trap the emitted light inside OLEDs.[83] Coupled with excitons, surface plasmons can cause increases in both radiation and non-radiative loss, depending on the size, interparticle distance of noble metal nanostructures, and spacing between noble metal nanostructure and emissive molecules.[84] When the distance between emissive molecules and the noble metal nanostructure is too small, non-radiative quenching of excitons occurs at the metal surface. Therefore, to maximize radiative enhancement by coupling between excitons and surface plasmons in OLEDs, the environment in which

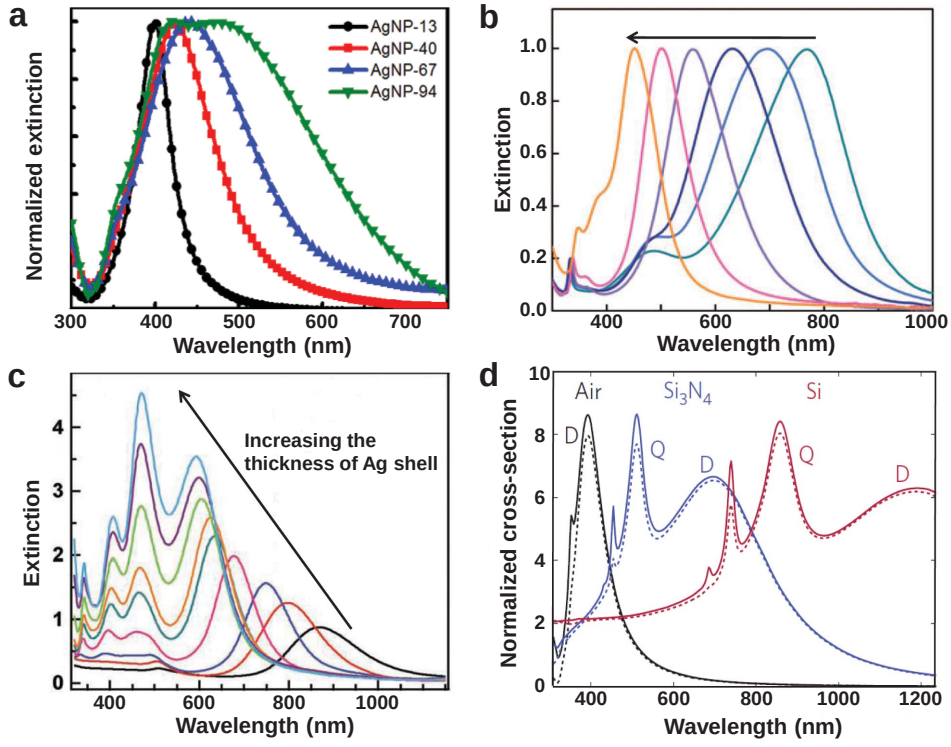

Figure 3. The change in plasmonic absorption properties of Ag NPs as a function of conditions: a–c) Extinction spectra of a) size-controlled Ag NPs (13–94 nm in diameter), b) Ag NPs with different edge sharpness (from Ag triangular nanoplates to circular disk), and c) Au–Ag core–shell nanorods with different thickness of Ag shell. d) Scattering cross-section spectra of Ag NPs (100 nm in diameter) embedded in different dielectric layers. Reproduced with permission: panel (a),[55] Copyright 2013, NPG; panel (b)[58] Copyright 2010, Wiley and (c),[62] Copyright 2012, Wiley; panel (d),[30] Copyright 2009, AIP.

noble metal nanostructures incorporate with emissive molecules in OLEDs should be optimized. Recently, the SPR effect of Ag NPs has been reported as a tool for improving the light emission and energy transfer in OLEDs.[49,50,85,86]

3.1. The Surface Plasmon Resonance Effect of Silver Nanoparticles-meditated Energy Transfer in OLEDs

The near-field enhancement by the SPR effect of Ag nanostructures can improve the energy transfer in OLEDs by enhancing the absorbance of donor molecules and emission of acceptor molecules. Electroluminescence in a top-emitting OLED has been increased by a factor of 10 by exploiting SPR effect-mediated radiative energy transfer through a 1D periodically corrugated Ag cathode SPR effect (**Figure 4**a).[85] The periodically corrugated Ag cathode was introduced by using holography lithography to create corrugations on a silica substrate, then depositing the anode, organic layers, and the Ag cathode. Then a dye-doped dielectric acceptor layer was deposited on top of the one-dimensionally corrugated Ag cathode. The acceptor layer was excited by the electroluminescence of a donor layer on the other side of the cathode. The energy transfer from the donor to acceptor was enhanced due to the coupled surface plasmons from the periodic corrugated Ag surface. Excitons generated in the emitting layer emit photons into surface plasmons at the interface between the corrugated Ag cathode and electron-transporting layer. These surface plasmons couple with the surface plasmons at the other interface between the Ag cathode and the acceptor layer. The acceptor is excited by the surface plasmons and releases its energy.

The SPR effect of Ag NPs can also be used to enhance energy transfer between donor and acceptor molecules in

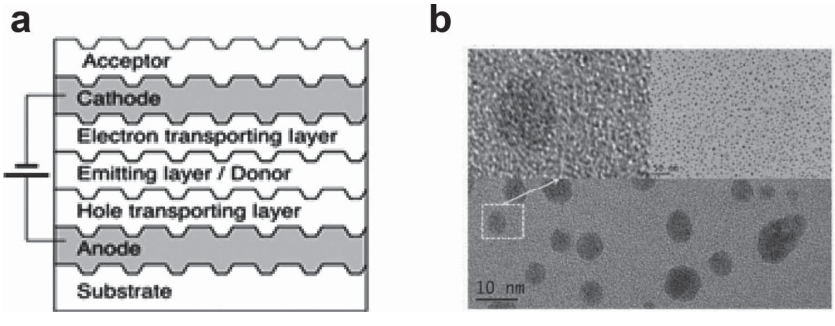

Figure 4. a) Schematic structure of the corrugated OLED with a one dimensionally periodic silver cathode, and b) transmission electron image (TEM) images of Ag nanoclusters by thermal evaporation. Reproduced with permission: panel (a),[85] Copyright 2008, American Institute of Physics; panel (b),[50] Copyright 2009, OSA.

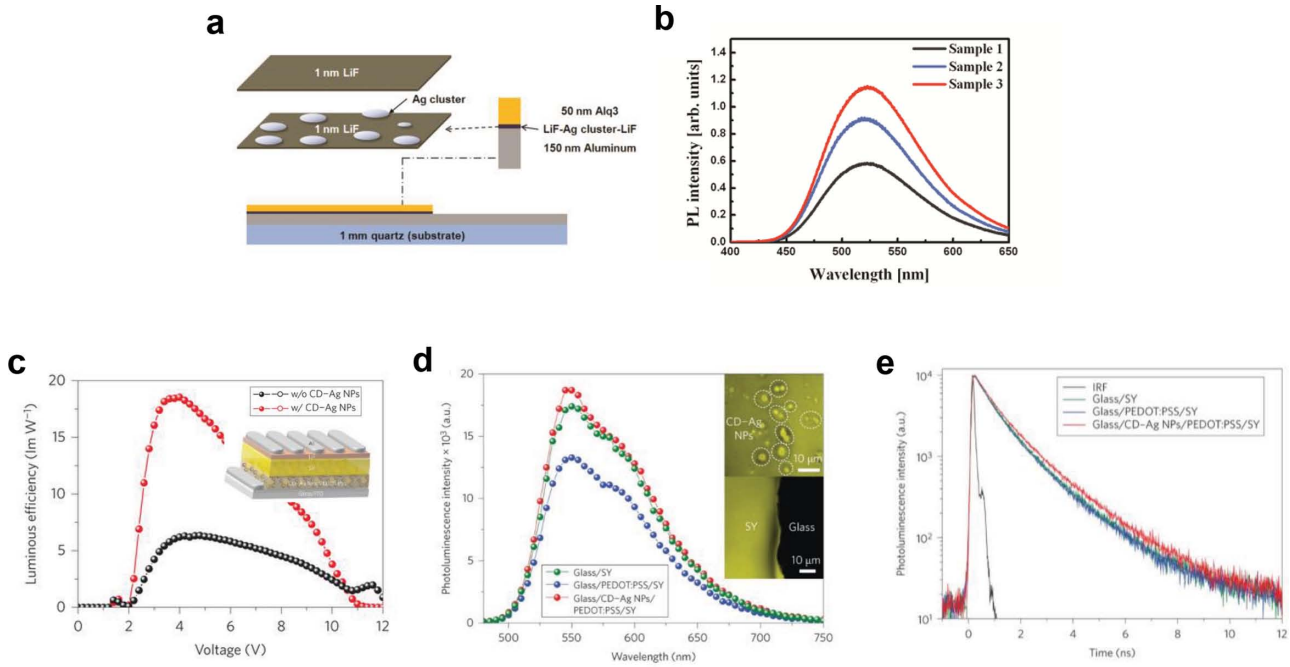

Figure 5. Emission properties of plasmonic OLEDs with Ag NPs: a) Schematic structure of the LiF/Al nanocluster/LiF cathode (inset: TEM image of Ag clusters on the LiF film). b) Photoluminescence spectra of samples 1–3 with the different Ag nanocluster densities. c) Luminous efficiency of PLEDs with and without CD-Ag NPs. The inset of Figure 5c is the device structure of plasmonic PLED with CD-Ag NPs. d) Steady-state photoluminescence spectra e) and photoluminescence decay profile of the super yellow film with and without CD-AgNPs. Reproduced with permission: panel (a) and (b),[49] Copyright 2009, American Institute of Physics; panel (c–e),[86] Copyright 2013, NPG.

OLEDs by exploiting the SPR effect of Ag NP-mediated FRET in fluorescent OLEDs that use tris-(8-hydroxyquinolinato) aluminum (Alq3) as a donor and 4-(dicyanomethylene)-2-methyl-6-(p-dimethyl-aminostyryl)-4H-pyran (DCM) as an acceptor.[50] To form a layer of Ag NPs, a very thin (<1 nm) Ag layer was deposited by thermal evaporation, and the size and spacing of Ag NPs was controlled by adjusting the mass thickness (Figure 4b). When the Ag NP with the SPR wavelength close to the wavelength of the donor emission were introduced, the donor decay rate increased. Additionally, when the SPR excitation energy approached the absorption range of the acceptor, the energy transfer between donor and acceptor was enhanced.

3.2. The Surface Plasmon Resonance Effect of Silver Nanoparticle-meditated Light Emission of OLEDs

Use of an LiF spacer can affect the interaction between the spontaneous exciton emission rate of a donor and the SPR effect of Ag NPs (**Figure 5**a).[49] Ag NP films were formed using thermal deposition, and Ag NPs of various size and density were deposited while controlling deposition rate and deposition thickness. The sample with the highest density had the highest PL emission intensity because of the dependency of the SPR effect on Ag NP cluster size and density (Figure 5b). To confirm the feasibility of the cathode structure, OLEDs with the following layer structure were fabricated using thermal vacuum evaporation: ITO/*N,N′*-di(naphtha-2-yl)-*N,N′*-diphenyl-benzidine/Alq_3/LiF/Ag cluster/LiF/Al. The OLED with LiF/Ag cluster/LiF-coated Al cathode showed slightly lower performance than the conventional LiF/Al cathode device due to the poor carrier injection caused by the high work function of LiF/Ag contact. However, the result showed the feasibility of utilizing surface plasmons.

Recently, highly efficient polymer light-emitting diodes (PLEDs) using Ag NPs have been reported.[87] Carbon dot-supported Ag NPs (CD-Ag NPs) were prepared using CD as both a template and reducing agent for Ag NPs and then spin-cast underneath conducting polymer, poly(3,4-ethylenedioxythiophene):polystyrene sulfonic acid (PEDOT:PSS). The ensemble plasmon coupling effect from clustering Ag NPs in CD-Ag NPs contributed to improving the radiative emission. The maximum luminous efficiencies of these PLED devices using poly(p-phenylene vinylene) copolymer, and Super Yellow (SY) for the emission layer were increased 6.33 lm W^{-1} to 18.54 lm W^{-1} after Ag NPs were incorporated with a conducting PEDOT:PSS anode (Figure 5c). These results were confirmed by the coincidence of the enhancements in the steady-state PL spectra and PL decay profile. Compared to the PEDOT:PSS/SY film without Ag NPs, that with Ag Ps had ≈30% higher PL intensity (Figure 5d), and longer average PL lifetime (Figure 5e).

4. Recent Progress in Plasmonic Polymer Solar Cells using Silver Nanoparticles

The performances of plasmonic PSCs have been gradually improved (**Table 2**) by employing different Ag NPs including nanoplates, nanoprisms, alloy NPs, and core–shell NPs, and incorporating these NPs into the electrode, charge transport

Table 1. Summary of device characteristics of plasmonic PSCs employing Ag NPs with different nanostructures and locations.

	Location	Nanostructures	Active layer	Initial PCE [%]	Final PCE [%]	Refs.
Inside	Electrode	Ag NPs	PTBT:$PC_{60}BM$	3.27	4.31	[6]
	PEDOT:PSS	Ag NPs	PTB7:$PC_{70}BM$	7.90	8.60	[49]
			PCDTBT:$PC_{70}BM$	6.40	7.60	
		Ag NPs	PTB7:$PC_{70}BM$	7.25	8.01	[85]
		Dual NPs (Ag+Au NPs)	PTB7:$PC_{70}BM$	7.25	8.67	
	TiO_2	Ag NPs (inverted)	PTB7:$PC_{70}BM$	6.23	7.52	[81]
	Active layer	Ag NPs	PCDTBT:$PC_{70}BM$	6.30	7.10	[88]
		Ag NPs	P3HT:$PC_{60}BM$	3.31	3.56	[87]
		Ag nanowires	P3HT:$PC_{60}BM$	3.31	3.91	
		Ag NPs	PCDTBT:$PC_{70}BM$	5.90	6.40	[88]
		Ag nanoplates	PCDTBT:$PC_{70}BM$	5.90	6.60	
		Ag nanoprisms	P3HT:$PC_{60}BM$	3.60	4.07	[36]
		Dual NPs (Ag NPs+prisms)	P3HT:$PC_{60}BM$	3.60	4.30	
		Ag–Au alloy NPs	P3HT:$PC_{60}BM$	3.61	4.73	[57]
Interface	ITO/ PEDOT:PSS	Ag nanodisks	P3HT:$PC_{60}BM$	2.72	3.46	[89]
		Ag–SiO_2 core–shell NPs	PTB7:$PC_{70}BM$	7.51	8.20	[58]
		CD–Ag NPs	PTB7:$PC_{70}BM$	7.53	8.31	[90]
	PEDOT:PSS/ active layer	Ag–SiO_2 core–shell NPs	PTB7:$PC_{70}BM$	7.51	8.92	[58]

layer, active layer, and the interface between them. Ag NPs with different sizes, shapes, structures, and elemental compositions have been explored to develop high-performance plasmonic PSCs. Because of solution-processability of Ag NPs, they can be easily applied to diverse positions within the devices, such as inside various layers (electrode, charge transport layer, and active layer) or at the interfaces between them (**Figure 6**a).

4.1. Silver Nanoparticles Inside the Layers

One approach has been reported for developing an ITO-free electrode using Ag NPs. Ag NPs were incorporated into PEDOT:PSS film to make a transparent conducting electrode instead of an ITO electrode and to use the SPR effect of Ag NPs at the same time.[6] The PCEs of these devices using a blend of poly(5,6-bis(octyloxy)-4-(thiophen-2-yl)benzo[c][1,2,5]thiadiazole) (PTBT) and [6,6]-phenyl-C_{60}-butyric acid methyl ester ($PC_{60}BM$) as the active layer were increased from 3.27% to 4.31% by introducing Ag NPs into the conducting PEDOT:PSS anode (Figure 6b). These Ag NPs contributed to the increase of electrical conductivity of PEDOT:PSS film and to the increase in light absorption by the active layer; these processes were confirmed by the coincidence of the enhancements in incident photon-to-current efficiency (IPCE) and absorption (Figure 6c).

Size-controlled Ag NPs were incorporated into a PEDOT:PSS hole transport layer by mixing Ag NPs and PEDOT:PSS and spin-casting this solution on top of an ITO substrate (Figure 6d).[55] Large Ag NPs have a tendency to increase both the ratio of total scattering power to the total absorption power, and the ratio of the forward scattering to the total scattering (Figure 6e). Ag NPs with a diameter of 67 nm in the PEDOT:PSS layer resulted in remarkable increases in PCEs from 6.4% to 7.6% for poly[N-9-heptadecanyl-2,7-carbazolealt-5,5-(4,7-di-2-thienyl-2,1,3-benzothiadiazole)] (PCDTBT): [6,6]-phenyl-C_{70}-butyric acid methyl ester ($PC_{70}BM$) devices, and from 7.9% to 8.6% for polythieno[3,4-b]thiophene/benzodithiophene (PTB7): $PC_{70}BM$ devices (Figure 6f). These improvements mostly resulted from increase in short-circuit current density (J_{SC}) by enhanced light absorption and forward scattering efficiency due to the SPR effect of Ag NPs.

Although most reports that use Ag NPs in PSC have used conventional PSCs, a few groups have attempted to develop inverted-type plasmonic PSCs that use Ag NPs. Using Ag NPs between molybdenium trioxide (MoO_3) buffer layers as the back-scattering centers, inverted PSCs (iPSCs) have been fabricated with the device configuration ITO/titanium oxide (TiO_2)/poly(3-hecylthiophene) (P3HT):$PC_{60}BM$/MoO_3/AgNPs/MoO_3/Ag, thereby improving PCEs from 2.70% to 3.35%.[91] Another design exploited the SPR effect by introducing Ag NPs into a TiO_2 buffer layer in iPSCs based on the PTB7:$PC_{70}BM$ active layer; optimized concentration of 30% Ag NPs in the TiO_2 layer led to ≈21% increase in PCE (from 6.23% to 7.52%) due to improved exciton generation rate and dissociation probability due to the SPR effect of Ag NPs.[92]

Recently, a mixture of Ag and Au NPs was introduced into the PEDOT:PSS layer to exploit the dual plasmonic effect of Ag and Au NPs (**Figure 7**a).[87] These mixed NPs effectively increased light absorption within the whole device architecture compared to those that used only Ag NPs or only Au NPs. The devices with dual NPs exhibited remarkable enhancement in PCEs of PTB7:$PC_{70}BM$ devices from 7.25% to 8.67% in comparison to the devices with single Ag NPs (8.01%) and Au NPs (8.16%) (Figure 7b).

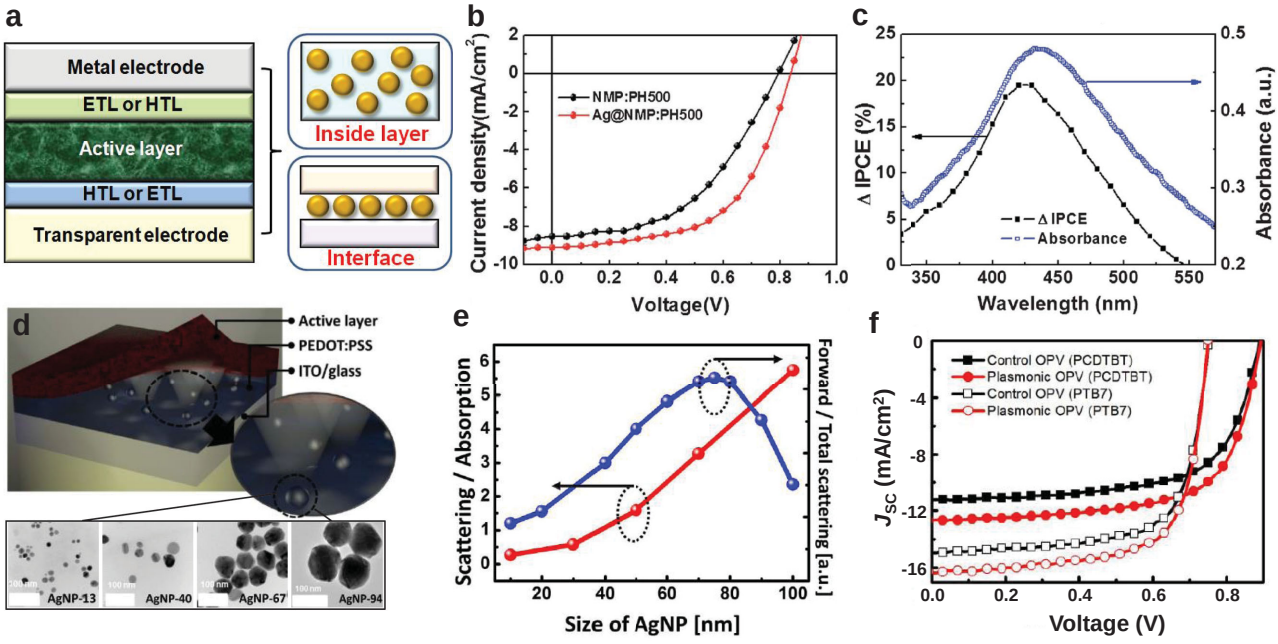

Figure 6. Designs of plasmonic PSCs with Ag NPs: a) Schematic illustration of plasmonic PSCs with Ag NPs inside various layers or at the interface between layers. b) *J–V* curves of PTBT:PC_{60}BM devices with NMP:PEDOT:PSS and Ag:NMP:PEDOT:PSS electrodes and c) comparison of enhanced IPCE and absorption by Ag NPs. d) device structure of the devices with size-controlled Ag NPs.[6] e) simulated ratio of scattering/absorption and forward scattering/total scattering as a function of size of Ag NPs. f) *J–V* curves of the PCDTBT:PC_{70}BM and PTB7:PC_{70}BM PSCs with optimized Ag NPs (67 nm in diameter).[55] Figures reproduced with permission: panel (b) and (c), Copyright 2013, RSC; panel (d–f), Copyright 2013, NPG.

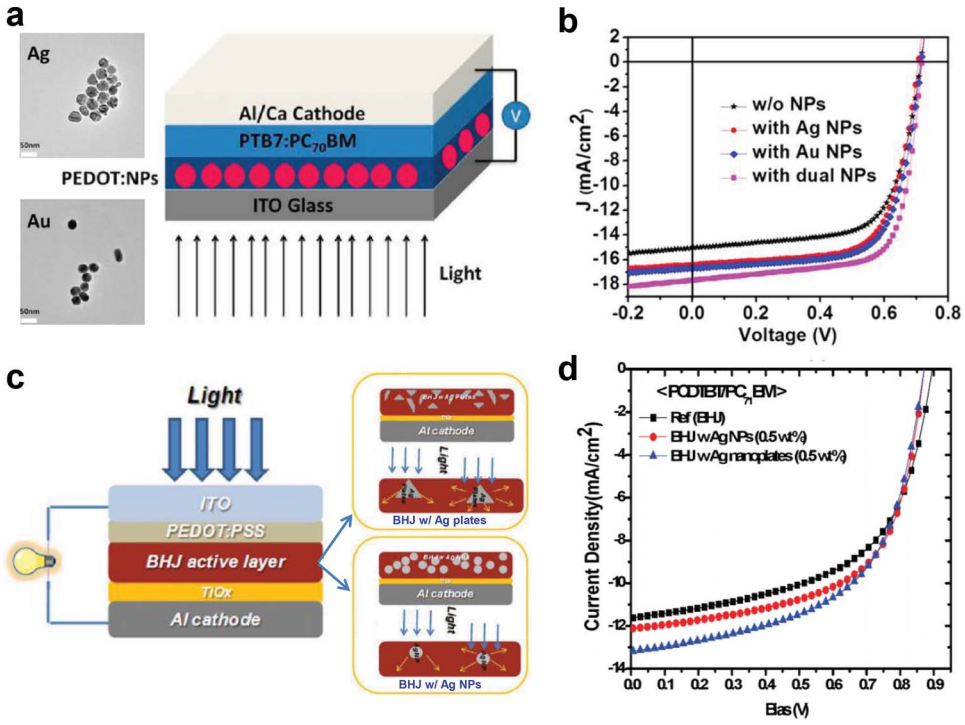

Figure 7. Introduction of Ag NPs into the buffer and active layer: a) Device structure and b) *J–V* curves of the PTB7:PC_{70}BM PSCs with both Ag and Au NPs embedded in PEDOT:PSS layer. c) Device structure and different scattering mechanisms of Ag NPs and Ag nanoplates inside the active layer. d) Comparison of *J–V* curves in the PCDTBT:PC_{70}BM devices with Ag NPs and Ag nanoplates. Reproduced with permission: panel (a) and (b),[87] Copyright 2013, ACS; panel (c) and (d),[93] Copyright 2012, RSC.

Direct contact between Ag NPs and the active layer can induce exciton quenching and recombination loss by non-radiative energy transfer.[29,35] When applying Ag NPs to an active layer, the surfaces of Ag NPs must be modified, and their size, concentration, and dispersion must be controlled. Ag NPs with different diameters (30, 40, and 60 nm) were synthesized using solution polyol chemistry, then incorporated directly into a bulk heterojunction (BHJ) active layer consisting of PCDTBT and $PC_{70}BM$;[88] the devices with 40 nm Ag NPs exhibited PCE improvement from 6.3% to 7.1% because the aggregated Ag clusters increased the efficiency of light trapping within the active layer and improved charge transport from BHJ films to the cathode.

Incorporating Ag NPs into P3HT:$PC_{60}BM$ BHJ film improves its structural stability. An Ag NP-free active layer exhibited both bulk reorganization indicated by increase in film thickness, and decreased degradation at the interface between the active layer and the PEDOT:PSS buffer layer under light exposure; in contrast, the layer with Ag NPs showed only minor degradation at the active/PEDOT:PSS interface.[89]

Shape-controlled Ag NPs can be applied to the active layer to improve device performance. Embedding 20 wt% of Ag nanowires (NWs) in a P3HT:$PC_{60}BM$ active layer increased PCEs from 3.31% to 3.91% by improving light absorption and charge-carrier mobilities.[90] Ag nanoplates blended into BHJ films increase optical path length by efficient scattering and light trapping in the active layer (Figure 7c)[93] and increased device efficiencies from 3.2% to 4.4% for P3HT:$PC_{70}BM$, and from 5.9% to 6.6% for PCDTBT:$PC_{70}BM$ (Figure 7d). When shape-controlled Ag NPs including Ag NPs and Ag nanoprisms were incorporated into the active layer, plasmonic peaks of Ag NPs and nanoprisms appeared at 420 and 600 nm, respectively.[39] The mixture of two different nanomaterials broadened the absorption spectrum over the whole visible wavelength region (350–750 nm), and optimized P3HT:$PC_{60}BM$ devices with Ag NPs and nanoprisms achieved the highest PCEs of 4.30% compared to those of the devices only with Ag NPs and Ag nanoprisms (reference: 3.60%, Ag NPs: 3.99%; Ag nanoprisms: 4.07%). Highly monodispersive large Au–Ag alloy NPs (diameter of ≈20 nm) with well-controlled composition were applied in a P3HT:$PC_{60}BM$ active layer;[60] optimized Au_{11}-Ag_{89} alloy NPs doped in the BHJ blend film achieved high PCE of 4.73%, whereas reference devices had PCE of 3.61%. These results were attributed to the alloy NPs acting as scattering centers for increasing light absorption and charge transport and reducing series resistance.

4.2. Silver Nanoparticles at the Interface Between the Layers

The Ag NPs have excellent dispersibility in alcoholic solvents, and can therefore be applied to any interfaces within devices such as ITO/PEDOT:PSS and PEDOT:PSS/active layer without removing the underlying layer. To maximize the SPR effect of Ag NPs in PSCs, the distance between Ag NPs and the active layer must be optimized. When this distance is too small, nonradiative decay causes exciton quenching; as the distance increases, the interaction between Ag NPs and active layer decreases exponentially. Therefore, Ag NPs have been commonly introduced at the interface between ITO and the PEDOT:PSS layer.[35,61,88] For example, Ag nanodisks were introduced into the ITO/PEDOT:PSS interface of P3HT:$PC_{60}BM$ PSCs by using electrostatic assembly (**Figure 8**a).[94] To make a positively charged ITO surface, the ITO substrates were immersed in poly(diallydimethylammonium chloride) solution. This modified ITO surface interacted electrostatically with negatively charged Ag nanodisks, leading to increased PCEs from 2.72% to 3.46% (Figure 8b).

CD–Ag NPs can be synthesized by irradiating UV light and using carbon dots both as reducing agent and template for Ag NPs (Figure 8c).[86] When applied at the interface between PEDOT:PSS and the active layer in PTB7:$PC_{70}BM$ PSCs, these CD-Ag NPs resulted in PCE improvement from 7.53% to 8.31%, which was attributed to broad light absorption by ensemble plasmon coupling caused by clustering of Ag NPs on the surface of carbon dots (Figure 8d).

Coating of metal NPs with dielectric materials can preserve the SPR effect of metal NPs by avoiding oxidation of metal core under air and by eliminating exciton quenching by direct contact between Ag NPs and active layer. When silica-coated Ag NPs (Ag@SiO_2) were introduced at the interfaces both of ITO/PEDOT:PSS (type I) and PEDOT:PSS/active layer (type II) (**Figure 9**a);[61] the change of Ag@SiO_2 location had strong effect on the dielectric constant of the surrounding matrix, leading to significant differences in electric field distribution and light absorption/scattering effect. PTB7:$PC_{70}BM$ devices with type II structure showed higher PCE of 8.92% than the devices without Ag@SiO_2 and with type I (Reference device: 7.51% and type I device: 8.20%) (Figure 9b). These results were attributed to strong coupling effect due to close distance between Ag NPs and the active layer, giving rise to additional light absorption and scattering effects over the broad region ranging from 400 to 700 nm (Figure 9c). Devices in which bare Ag NPs were used instead of Ag@SiO_2 were fabricated for comparison. The type I devices showed 10% increase in PCE, whereas poor device performance was obtained in type II devices. These results imply that silica shells contribute to preventing exciton quenching and that they enable light absorption and scattering that enhance device performance in the type II device structure.

5. Conclusion

The development of new materials and device architectures has contributed to great progress in the efficiencies of organic optoelectronic devices. Unique properties of Ag NPs enable them to be easily applied inside various layers or at the interface between layers, and their SPR effect effectively increases light trapping or extraction efficiency and improves energy transfer between donor and acceptor molecules, further enhancing device performances. Although the efficiencies of plasmonic OLEDs and PSCs are still lower than those of inorganic material-based devices, Ag NPs may offer the potential to achieve high-efficiency OLEDs and PSCs by combining active materials and device structures. Basically, attaining extremely high performance of plasmonic OLEDs and PSCs requires development of novel Ag NPs with optimum size, shape, and composition for broad absorption or extraction and energy transfer

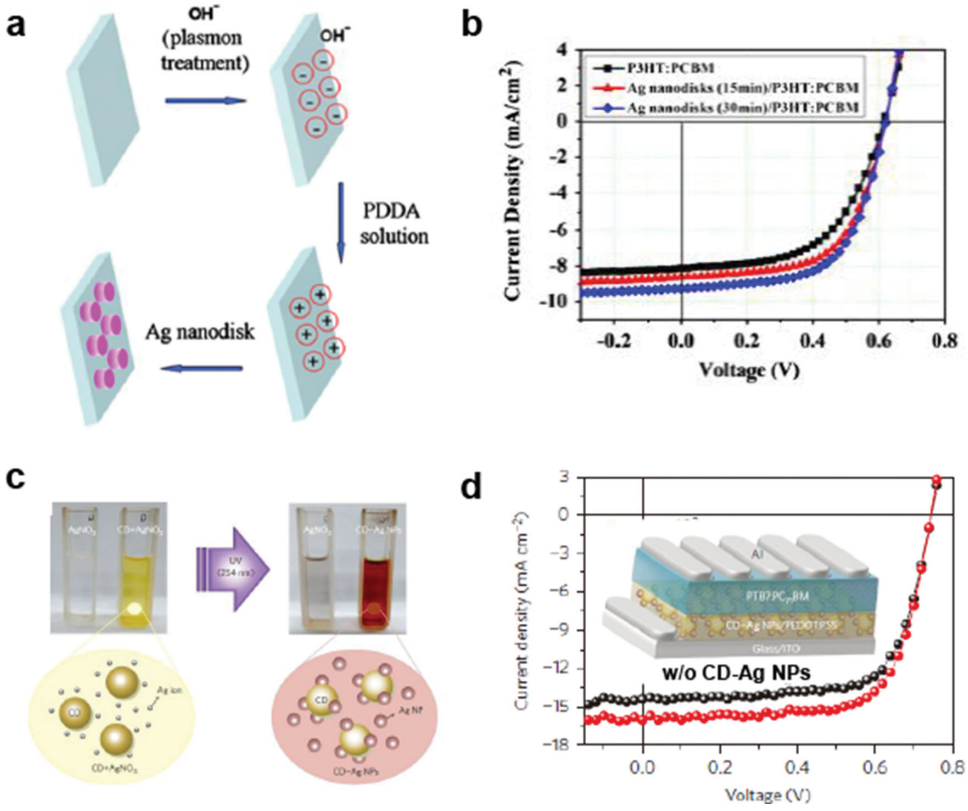

Figure 8. Introduction of Ag NPs at the interface between ITO and buffer layer: a) Fabrication of electrostatic self-assembled layer of Ag nanodisks and b) *J–V* curves of P3HT:$PC_{60}BM$ PSCs with different size of Ag nanodisks (15 and 30 nm in diameter). c) Real images and schematic illustration for synthesis of CD-Ag NPs and d) *J–V* curves of PTB7:$PC_{70}BM$ PSCs with CD-Ag NPs (inset: device structure with CD-Ag NPs). Reproduced with permission: panel (a) and (b),[94] Copyright 2011, Elsevier; panel (c) and (d),[86] Copyright 2013, NPG.

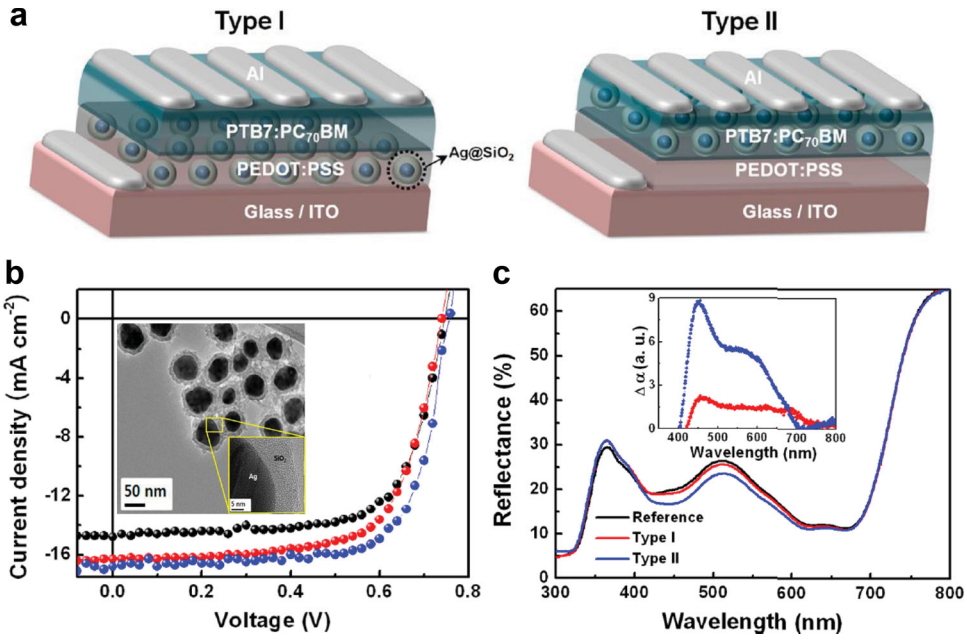

Figure 9. Introduction of Ag NPs at the interface between buffer and active layers: a) Device structures and b) *J–V* curves of PTB7:$PC_{70}BM$ PSCs with type I (ITO/Ag@SiO_2/PEDOT:PSS) and type II (ITO/PEDOT:PSS/Ag@SiO_2/PTB7:$PC_{70}BM$) (inset: transmission electron image (TEM) of Ag@SiO_2). The diameter of Ag core and thickness of SiO_2 shell are ≈50 and ≈10 nm, respectively. c) Reflectance spectra of these devices with different locations of Ag@SiO_2 (inset: absorption enhancement by Ag@SiO_2 in the devices with type I and II structure.) Reproduced with permission.[61] Copyright 2013, ACS.

enhancement, and effective device architectures for improving device performance.

Acknowledgements

S.-H.J. and H.C. contributed equally to this work. This work was supported by the National Research Foundation of Korea (NRF) grant funded by the Korea government (MSIP) (NRF-2013R1A2A2A01068753, NRF-2013R1A2A2A01015342). S.-H.J. gratefully acknowledges financial support by Global PH.D Fellowship Program through the National Research Foundation of Korea (NRF) funded by the Ministry of Education (NRF-2012H1A2A1002581).

Received: May 28, 2014
Revised: July 20, 2014
Published online: September 5, 2014

[1] M. S. White, M. Kaltenbrunner, E. D. Glowacki, K. Gutnichenko, G. Kettlgruber, I. Graz, S. Aazou, C. Ulbricht, D. A. M. Egbe, M. C. Miron, Z. Major, M. C. Scharber, T. Sekitani, T. Someya, S. Bauer, N. S. Sariciftci, *Nat. Photonics* **2013**, *7*, 811.
[2] M. Vosgueritchian, D. J. Lipomi, Z. Bao, *Adv. Funct. Mater.* **2012**, *22*, 421.
[3] G. Yu, J. Gao, J. C. Hummelen, F. Wudl, A. J. Heeger, *Science* **1995**, *270*, 1789.
[4] S. Günes, H. Neugebauer, N. S. Sariciftci, *Chem. Rev.* **2007**, *107*, 1324.
[5] C. E. Small, S. Chen, J. Subbiah, C. M. Amb, S.-W. Tsang, T.-H. Lai, J. R. Reynolds, F. So, *Nat. Photonics* **2012**, *6*, 115.
[6] S.-J. Ko, H. Choi, W. Lee, T. Kim, B. R. Lee, J.-W. Jung, J.-R. Jeong, M. H. Song, J. C. Lee, H. Y. Woo, J. Y. Kim, *Energy Environ. Sci.* **2013**, *6*, 1949.
[7] L. Dou, J. You, J. Yang, C.-C. Chen, Y. He, S. Murase, T. Moriarty, K. Emery, G. Li, Y. Yang, *Nat. Photonics* **2012**, *6*, 180.
[8] R. F. Service, *Science* **2011**, *332*, 293.
[9] J. Y. Kim, K. Lee, N. E. Coates, D. Moses, T.-Q. Nguyen, M. Dante, A. J. Heeger, *Science* **2007**, *317*, 222.
[10] J. K. Lee, W. L. Ma, C. J. Brabec, J. Yuen, J. S. Moon, J. Y. Kim, K. Lee, G. C. Bazan, A. J. Heeger, *J. Am. Chem. Soc.* **2008**, *130*, 3619.
[11] Y. Liang, Z. Xu, J. Xia, S.-T. Tsai, Y. Wu, G. Li, C. Ray, L. Yu, *Adv. Mater.* **2010**, *22*, E135.
[12] J. Y. Kim, S. H. Kim, H. H. Lee, K. Lee, W. Ma, X. Gong, A. J. Heeger, *Adv. Mater.* **2006**, *18*, 572.
[13] H. Choi, J. S. Park, E. Jeong, G.-H. Kim, B. R. Lee, S. O. Kim, M. H. Song, H. Y. Woo, J. Y. Kim, *Adv. Mater.* **2011**, *23*, 2759.
[14] K. Yamae, H. Tsuji, V. Kittichungchit, N. Ide, T. Komoda, *SID 13 Digest* **2013**, 916.
[15] I. S. Oh, G. M. Kim, S. H. Han, S. Y. Oh, *Electron. Mater, Lett.* **2013**, *9*, 375.
[16] J. H. Kim, J.-Y. Cho, J. Park, B. K. Lee, K.-H. Baek, H. Lee, L.-M. Do, *Electron. Mater, Lett.* **2014**, *10*, 27.
[17] K. Sugi, T. Ono, D. Kato, T. Yonehara, T. Sawabe, S. Enomoto, I. Amemiya, *SID 12 Digest* **2012**, 1548.
[18] H. S. Kim, C. K. Kim, H. W. Jang, *Electron. Mater. Lett.* **2013**, *9*, 39.
[19] C. Adachi, M. A. Baldo, M. E. Thompson, S. R. Forrest, *J. Appl. Phys.* **2001**, *90*, 5048.
[20] C. F. Madigan, M. H. Lu, J. C. Sturm, *Appl. Phys. Lett.* **2000**, *76*, 1650.
[21] P. E. Shaw, A. Ruseckas, I. D. W. Samuel, *Adv. Mater.* **2008**, *20*, 3516.
[22] Y. Mei, M. A. Loth, M. Payne, W. Zhang, J. Smith, C. S. Day, S. R. Parkin, M. Heeney, I. McCulloch, T. D. Anthopoulos, J. E. Anthony, O. D. Jurchescu, *Adv. Mater.* **2013**, *25*, 4352.
[23] U. Zschieschang, F. Ante, T. Yamamoto, K. Takimiya, H. Kuwabara, M. Ikeda, T. Sekitani, T. Someya, K. Kern, H. Klauk, *Adv. Mater.* **2010**, *22*, 982.
[24] I. McCulloch, M. Heeney, C. Bailey, K. Genevicius, I. MacDonald, M. Shkunov, D. Sparrowe, S. Tierney, R. Wagner, W. Zhang, M. L. Chabinyc, R. J. Kline, M. D. McGehee, M. F. Toney, *Nat. Mater.* **2006**, *5*, 328.
[25] T. Sakanoue, H. Sirringhaus, *Nat. Mater.* **2010**, *9*, 736.
[26] E. Orgiu, A. M. Masillamani, J.-O. Vogel, E. Treossi, A. Kiersnowski, M. Kastler, W. Pisula, F. Dotz, V. Palermo, P. Samori, *Chem. Commun.* **2012**, *48*, 1562.
[27] P. W. M. Blom, V. D. Mihailetchi, L. J. A. Koster, D. E. Markov, *Adv. Mater.* **2007**, *19*, 1551.
[28] D. E. Markov, E. Amsterdam, P. W. M. Blom, A. B. Sieval, J. C. Hummelen, *J. Phys. Chem. A* **2005**, *109*, 5266.
[29] Q. Gan, F. J. Bartoli, Z. H. Kafafi, *Adv. Mater.* **2013**, *25*, 2385.
[30] H. A. Atwater, A. Polman, *Nat. Mater.* **2010**, *9*, 205.
[31] S. Linic, P. Christopher, D. B. Ingram, *Nat. Mater.* **2011**, *10*, 911.
[32] A. P. Kulkarni, K. M. Noone, K. Munechika, S. R. Guyer, D. S. Ginger, *Nano Lett.* **2010**, *10*, 1501.
[33] E. Hutter, J. H. Fendler, *Adv. Mater.* **2004**, *16*, 1685.
[34] A. Kumar, R. Srivastava, P. Tyagi, D. S. Mehta, M. N. Kamalasanan, *Org. Electron.* **2012**, *13*, 159.
[35] D. H. Wang, D. Y. Kim, K. W. Choi, J. H. Seo, S. H. Im, J. H. Park, O. O. Park, A. J. Heeger, *Angew. Chem. Int. Ed.* **2011**, *50*, 5519.
[36] J.-L. Wu, F.-C. Chen, Y.-S. Hsiao, F.-C. Chien, P. Chen, C.-H. Kuo, M. H. Huang, C.-S. Hsu, *ACS Nano* **2011**, *5*, 959967.
[37] Y.-S. Hsiao, S. Charan, F.-Y. Wu, F.-C. Chien, C.-W. Chu, P. Chen, F.-C. Chen, *J. Phys. Chem. C* **2012**, *116*, 20731.
[38] X. Chen, B. Jia, J. K. Saha, B. Cai, N. Stokes, Q. Qiao, Y. Wang, Z. Shi, M. Gu, *Nano Lett.* **2012**, *12*, 2187.
[39] X. Li, W. C. H. Choy, H. Lu, W. E. I. Sha, A. H. P. Ho, *Adv. Funct. Mater.* **2013**, *23*, 2728.
[40] M. Rycenga, C. M. Cobley, J. Zeng, W. Li, C. H. Moran, Q. Zhang, D. Qin, Y. Xia, *Chem. Rev.* **2011**, *111*, 3669.
[41] P. Mulvaney, *Langmuir* **1996**, *12*, 788.
[42] E. C. Le Ru, P. G. Etchegoin, in *Principles of Surface-Enhanced Raman Spectroscopy*, Elsevier, Oxford, UK **2009**.
[43] M. Perner, P. Bost, U. Lemmer, G. von Plessen, J. Feldmann, U. Becker, M. Mennig, M. Schmitt, H. Schmidt, *Phys. Rev. Lett.* **1997**, *78*, 2192.
[44] H. Wang, F. Tam, N. K. Grady, N. J. Halas, *J. Phys. Chem. B* **2005**, *109*, 18218.
[45] M. Heo, H. Cho, J.-W. Jung, J.-R. Jeong, S. Park, J. Y. Kim, *Adv. Mater.* **2011**, *23*, 5689.
[46] R. C. Ropp, *Luminescence and the Solid State*, Elsevier, Amsterdam **1991**.
[47] L. Zhao, T. Ming, L. Shao, H. Chen, J. Wang, *J. Phys. Chem. C* **2012**, *116*, 8287.
[48] H.-J. Park, D. Vak, Y.-Y. Noh, B. Lim, D.-Y. Kim, *Appl. Phys. Lett.* **2007**, *90*, 161107.
[49] K. Y. Yang, K. C. Choi, C. W. Ahn, *Appl. Phys. Lett.* **2009**, *94*, 173301.
[50] K. Y. Yang, K. C. Choi, C. W. Ahn, *Opt. Express* **2009**, *17*, 11495.
[51] Y.-C. Fang, L. Hong, L. Wan, K.-X. Zhang, X. Lu, C.-M. Wang, J. Yang, X.-l. Xu, *J. Vac. Sci. Technol. A* **2013**, *31*, 041401.
[52] K. H. Cho, S. I. Ahn, S. M. Lee, S. M. Lee, C. S. Choi, K. C. Choi, *Appl. Phys. Lett.* **2010**, *97*, 193306.
[53] J. R. Lakowicz, *Principles of Fluorescence Spectroscopy*, Springer, MD **2009**.
[54] S. Tabassum, W. M. Al-Asbahy, M. Afzal, F. Arjmand, R. H. Khan, *Mol. BioSyst.* **2012**,*8*, 2424.
[55] S.-W. Baek, J. Noh, C.-H. Lee, B. Kim, M.-K. Seo, J.-Y. Lee, *Sci. Rep.* **2013**, *3*, 1726.

[56] K.-C. Lee, S.-J. Lin, C.-H. Lin, C.-S. Tsai, Y.-J. Lu, *Surf. Coat. Technol.* **2008**, *202*, 5339.
[57] Y. Xia, Y. Xiong, B. Lim, S. E. Skrabalak, *Angew. Chem. Int. Ed.* **2009**, *48*, 60.
[58] J. Zeng, S. Roberts, Y. Xia, *Chem. Euro. J.* **2010**, *16*, 12559.
[59] B. J. Wiley, S. H. Im, Z.-Y. Li, J. McLellan, A. Siekkinen, Y. Xia, *J. Phys. Chem. B* **2006**, *110*, 15666.
[60] H.-C. Chen, S.-W. Chou, W.-H. Tseng, I. W. P. Chen, C.-C. Liu, C. Liu, C.-L. Liu, C.-h. Chen, C.-I. Wu, P.-T. Chou, *Adv. Funct. Mater.* **2012**, *22*, 3975.
[61] H. Choi, J.-P. Lee, S.-J. Ko, J.-W. Jung, H. Park, S. Yoo, O. Park, J.-R. Jeong, S. Park, J. Y. Kim, *Nano Lett.* **2013**, *13*, 2204.
[62] R. Jiang, H. Chen, L. Shao, Q. Li, J. Wang, *Adv. Mater.* **2012**, *24*, OP200.
[63] G. Xu, M. Tazawa, P. Jin, S. Nakao, K. Yoshimura, *Appl. Phys. Lett.* **2003**, *82*, 3811.
[64] H. Mertens, J. Verhoeven, A. Polman, F. D. Tichelaar, *Appl. Phys. Lett.* **2004**, *85*, 1317.
[65] F. J. Beck, A. Polman, K. R. Catchpole, *J. Appl. Phys.* **2009**, *105*, 114310.
[66] Q. Zhang, W. Li, C. Moran, J. Zeng, J. Chen, L.-P. Wen, Y. Xia, *J. Am. Chem. Soc.* **2010**, *132*, 11372.
[67] C. Kealley, M. Cortie, *Plasmonics* **2010**, *5*, 37.
[68] Y. Sun, B. Wiley, Z.-Y. Li, Y. Xia, *J. Am. Chem. Soc.* **2004**, *126*, 9399.
[69] J. Chen, B. Wiley, J. McLellan, Y. Xiong, Z.-Y. Li, Y. Xia, *Nano Lett.* **2005**, *5*, 2058.
[70] W. He, X. Wu, J. Liu, K. Zhang, W. Chu, L. Feng, X. Hu, W. Zhou, S. Xie, *Langmuir* **2009**, *26*, 4443.
[71] S. E. Skrabalak, J. Chen, Y. Sun, X. Lu, L. Au, C. M. Cobley, Y. Xia, *Acc. Chem. Res.* **2008**, *41*, 1587.
[72] R. G. Sanedrin, D. G. Georganopoulou, S. Park, C. A. Mirkin, *Adv. Mater.* **2005**, *17*, 1027.
[73] Z. Y. Li, J. Yuan, Y. Chen, R. E. Palmer, J. P. Wilcoxon, *Appl. Phys. Lett.* **2005**, *87*, 243103.
[74] P. R. Selvakannan, A. Swami, D. Srisathiyanarayanan, P. S. Shirude, R. Pasricha, A. B. Mandale, M. Sastry, *Langmuir* **2004**, *20*, 7825.
[75] S. Mandal, P. R. Selvakannan, R. Pasricha, M. Sastry, *J. Am. Chem. Soc.* **2003**, *125*, 8440.
[76] T. Nakamura, Y. Tsukahara, T. Yamauchi, T. Sakata, H. Mori, Y. Wada, *Chem. Lett.* **2007**, *36*, 154.
[77] M. Tsuji, S. Hikino, R. Tanabe, D. Yamaguchi, *Chem. Lett.* **2010**, *39*, 334.
[78] D.-K. Lim, I.-J. Kim, J.-M. Nam, *Chem. Commun.* **2008**, 5312.
[79] M. Kahraman, Ö. Aydın, M. Çulha, *Plasmonics* **2009**, *4*, 293.
[80] M. Ohmori, E. Matijević, *J. Colloid Interface Sci.* **1993**, *160*, 288.
[81] D. V. Goia, E. Matijevic, *New J. Chem.* **1998**, *22*, 1203.
[82] C. W. Tang, S. A. VanSlyke, *Appl. Phys. Lett.* **1987**, *51*, 913.
[83] A. Chutinan, K. Ishihara, T. Asano, M. Fujita, S. Noda, *Org. Electron.* **2005**, *6*, 3.
[84] J. C. Ostrowski, A. Mikhailovsky, A. Bussian, M. A. Summers, S. K. Buratto, G. C. Bazan, *Adv. Funct. Mater.* **2006**, *16*, 1221.
[85] J. Feng, T. Okamoto, R. Naraoka, S. Kawata, *Appl. Phys. Lett.* **2008**, *93*051106.
[86] H. Choi, S.-J. Ko, Y. Choi, P. Joo, T. Kim, B. R. Lee, J.-W. Jung, H. J. Choi, M. Cha, J.-R. Jeong, I.-W. Hwang, M. H. Song, B.-S. Kim, J. Y. Kim, *Nat. Photonics* **2013**, *7*, 732.
[87] H. Choi, S.-J. Ko, Y. Choi, P. Joo, T. Kim, B. R. Lee, J.-W. Jung, H. J. Choi, M. Cha, J.-R. Jeong, I.-W. Hwang, M. H. Song, B.-S. Kim, J. Y. Kim, *Nat. Photonics* **2013**, *7*, 732.
[88] D. H. Wang, K. H. Park, J. H. Seo, J. Seifter, J. H. Jeon, J. K. Kim, J. H. Park, O. O. Park, A. J. Heeger, *Adv. Energy Mater.* **2011**, *1*, 766.
[89] B. Paci, G. D. Spyropoulos, A. Generosi, D. Bailo, V. R. Albertini, E. Stratakis, E. Kymakis, *Adv. Funct. Mater.* **2011**, *21*, 3573.
[90] C.-H. Kim, S.-H. Cha, S. C. Kim, M. Song, J. Lee, W. S. Shin, S.-J. Moon, J. H. Bahng, N. A. Kotov, S.-H. Jin, *ACS Nano* **2011**, *5*, 3319.
[91] P. Xu, L. Shen, F. Meng, J. Zhang, W. Xie, W. Yu, W. Guo, X. Jia, S. Ruan, *Appl. Phys. Lett.* **2013**, *102*, 123301.
[92] M.-F. Xu, X.-Z. Zhu, X.-B. Shi, J. Liang, Y. Jin, Z.-K. Wang, L.-S. Liao, *ACS Appl. Mater. Interfaces* **2013**, *5*, 2935.
[93] D. H. Wang, J. K. Kim, G.-H. Lim, K. H. Park, O. O. Park, B. Lim, J. H. Park, *RSC Adv.* **2012**, *2*, 7268.
[94] J. Pei, J. Tao, Y. Zhou, Q. Dong, Z. Liu, Z. Li, F. Chen, J. Zhang, W. Xu, W. Tian, *Sol. Energy Mater. Sol. Cells* **2011**, *95*, 3281.